Exp Fluids (2010) 48:577–587
DOI 10.1007/s00348-010-0824-1

RESEARCH ARTICLE

Interfacial PIV to resolve flows in the vicinity of curved surfaces

Chuong V. Nguyen · Thien D. Nguyen · John C. Wells · Akihiko Nakayama

Received: 1 October 2008 / Revised: 7 January 2010 / Accepted: 11 January 2010 / Published online: 9 February 2010

Abstract PIV measurements near a wall are generally difficult due to low seeding density, low velocity, high velocity gradient, and strong reflections. Such problems are often compounded by curved boundaries, which are commonly found in many industrial and medical applications. To systematically solve these problems, this paper presents two novel techniques for near-wall measurement, together named Interfacial PIV, which extracts both wall-shear gradient and near-wall tangential velocity profiles at one-pixel resolution. To deal with curved walls, image strips at a curved wall are stretched into rectangles by means of conformal transformation. To extract the maximal spatial information on the near-wall tangential velocity field, a novel 1D correlation function is performed on each horizontal pixel line of the transformed image template to form a "correlation stack". This 1D correlation function requires that the wall-normal displacement component of the particles be smaller than the particle image diameter in order to produce a correlation signal. Within the image regions satisfying this condition, the correlation function yields peaks that form a tangential velocity profile. To determine this profile robustly, we propose to integrate gradients of tangential velocity outward from the wall, wherein the gradient at each wall-normal position is measured by fitting a straight line to the correlation peaks. The capability of Interfacial PIV was validated against Particle Image Distortion using synthetic image pairs generated from a DNS velocity field over a sinusoidal bed. Different velocity measurement schemes performed on the same correlation stacks were also demonstrated. The results suggest that Interfacial PIV using line fitting and gradient integration provides the best accuracy of all cases in the measurements of velocity gradient and velocity profile near wall surfaces.

C. V. Nguyen (✉)
Fluid Laboratory for Aeronautical and Industrial Research,
Department of Mechanical and Aerospace Engineering,
Monash University, Clayton, Melbourne, VIC 3800, Australia
e-mail: chuong.nguyen@eng.monash.edu.au

T. D. Nguyen · J. C. Wells
Department of Civil & Environmental Engineering,
Ritsumeikan University, Shiga, Japan
e-mail: gr044050@se.ritsumei.ac.jp

J. C. Wells
e-mail: jwells@se.ritsumei.ac.jp

A. Nakayama
Department of Civil Engineering,
Kobe University, Hyogo, Japan
e-mail: nakayama@kobe-u.ac.jp

1 Introduction

The important roles of wall-shear gradients and the flow field immediately adjacent to the wall in vorticity generation, and in heat and mass transfer have attracted the interest of many researchers. However, performing PIV measurements very near walls requires care to reduce the erroneous velocity vectors due to high-shear gradients and wall reflections.

Concerning high-shear regions, where tracer patterns deform and reduce cross-correlation signal, Huang et al. (1993) proposed Particle Image Distortion (PID) which distorts a particle image according to the velocity field initially measured by standard cross-correlation to iteratively compensate the estimated deformation. To completely remove the effects of particle pattern deformation, Westerweel et al. (2004) proposed a single-pixel resolution PIV technique which, however, applies time-averaging

over hundreds of image pairs and is therefore mainly applicable to steady flows such as micro flows.

In order to improve the velocity measurements in the near-wall region, several techniques have been developed. To remove the biasing effect of the wall image from the correlation function, Gui et al. (2000) proposed a digital mask technique where the correlation function includes a binary mask to remove correlation signal from the solid region of a template. The locations of calculated velocity vectors are usually chosen to be at the center of the templates. However, for templates that partly include the non-fluid region or the wall boundary, the resulting vector locations are clearly suboptimal for representing the fluid flow. For such image templates, Hochareon and Fontaine (2004) proposed to relocate the displacement vector to the centroid of the fluid region, instead of the center of the interrogation window. Nguyen and Wells (2006b) proposed a technique called "PIV/Interface Gradiometry" or "PIV/IG" to directly measure the wall velocity gradients by shearing the PIV image templates parallel to a no-slip wall and to perform stereo reconstruction of the wall-shear gradients. This technique achieves higher measurement accuracy of velocity gradient than velocity differentiation. To better deal with curved wall boundaries and near-wall velocity fields, Nguyen and Wells (2006a) proposed some extensions to PIV/IG, including a conformal transformation of particle images and a new correlation function. The new correlation function produces a 1D "correlation stack", instead of a standard 2D correlation map. This technique can provide instantaneous near-wall velocity profiles with single-pixel resolution in the wall-normal direction. An increase in velocity resolution near the wall for turbulent flows was also achieved by Theunissen et al.'s (2008) adaptive concept in which the template aspect ratio varies when close to the wall while the number of particles in the image template is kept constant and the image template is additionally rotated parallel to the boundary to exclude the interface from the correlation process.

This paper will generalize the technique to resolve flows near curved boundaries initially proposed by Nguyen and Wells (2006a). Additionally, this paper presents a novel technique to directly obtain the wall-shear velocity gradient and the tangential velocity profile from the correlation stack. Investigations using synthetic and experimental PIV images of turbulent flow over a wavy bed as shown in Fig. 1 are performed to demonstrate the capabilities of Interfacial PIV to measure wall-shear gradient and near-wall velocity profiles. We will refer to this generalized technique as "Interfacial PIV" or "IPIV". In addition to standard channel flow like that examined herein, IPIV has already proven itself suitable for in-vitro measurement of the wall-shear gradient of a flow in a modeled carotid artery, as carried out by Buchmann et al. (2008, 2009).

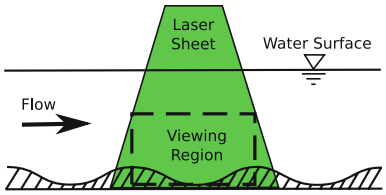

Fig. 1 A schematic drawing of an open-channel flow over a wavy bed

2 Interfacial PIV

Building on our previous work (Nguyen and Wells 2006a), the new IPIV method consists of 5 steps:

1. Identifying the position of the wall boundary
2. Conformally transforming the near-wall image region to a rectangular shape to handle sloping and/or curved wall boundaries
3. Calculating line correlations between the first and second exposures to obtain a "stack" of 1D-correlations
4. Measuring the wall-shear velocity gradient and deriving tangential velocity profile from the correlation stack
5. Reverse transforming the velocity profile and wall-shear gradient obtained in transformed domain to physical domain.

Within this recipe, steps 3 and 4 can be optionally replaced by any suitable PIV processing, i.e., Particle Image Distortion as shown later on. Subsequent sections are detailed descriptions of the earlier mentioned steps, exemplified by an experimental test and by the synthetic images that will be detailed in Sect. 3.

2.1 Identifying wall boundary

The accuracy of wall identification strongly affects the accuracy of the IPIV technique when the boundary condition is assumed to be no-slip (Nguyen et al. 2006). Based on our experience so far, an edge detection algorithm by Marr and Hildreth (1980) seems to work the best for our experimental images, where there is a strong intensity difference between the wall region and the fluid region. This algorithm starts with image smoothing using a Gaussian filter. Then, the Laplacian of the image is calculated and the wall boundary is considered as zero-crossing points.

In this paper, we identify the wall in a time-averaged image $I_{avg}(x, y)$ with an assumption of fixed boundary. The smoothed image is a result of the convolution between the wall image $I_{avg}(x, y)$ and a Gaussian filter $g(x, y)$:

$$s(x, y) = I_{avg}(x, y) \times g(x, y) \quad (1)$$

By using the derivative rule for convolution, the Laplacian of the smoothed image $s(x, y)$ can be calculated rapidly as the convolution between the averaged image and the Laplacian of the filter:

$$\nabla^2 s(x, y) = I_{avg}(x, y) \times \nabla^2 g(x, y) \quad (2)$$

The wall boundary obtained from the zero-crossing points of the Laplacian must, however, be filtered or curve-fitted to obtain a continuous boundary for conformal transformation. In our case of the sinusoidal wall, Fourier filtering yielded a better accuracy than other functions such as polynomial functions. The standard deviation value of the Gaussian filter $g(x, y)$ that yielded good detection accuracy was, in our case, from 1 to 5 pixels; for values greater than 9 pixels, there was a large discrepancy between the detected and the actual wall locations. Fig. 2 exemplifies the detected boundary from experimental images of a water channel with a sinusoidal wall.

2.2 Conformally transforming near-wall region to rectangle

Next, we apply conformal transformation to convert the near-wall image region, named physical domain (x, y), to a rectangular image region, named transformed domain (ξ, η).

Conformal transformation is a mapping function which preserves angles. Therefore, it has the advantages of preserving the orthogonality of the fluid volume and simplifying the transformation of measured velocity field. In near-wall velocity measurements, a local coordinate system $(\tilde{x}, \tilde{y})$ aligned to the wall surface is often used to express important local flow properties such as wall-shear gradient and near-wall velocity profile. However, as the local coordinate system varies along a curved wall, it is easier to obtain the local flow properties by computing them from the transformed domain and then reverse transforming back to the physical domain.

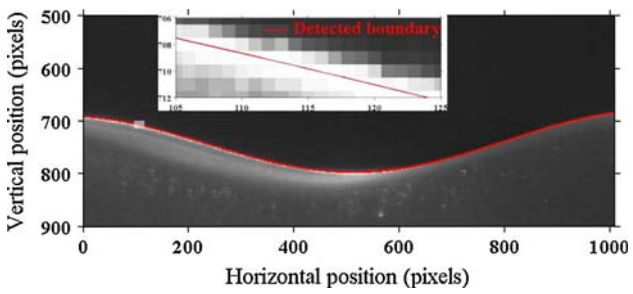

Fig. 2 Detected boundary by Laplacian of Gaussian method, with closeup of white rectangle, plotted on time-averaged experimental image

The conformal transformation described in this paper is based on a conformal mapping and grid generation algorithm by Ives and Zacharias (1987). The region in the physical domain to be transformed must be bounded by four contours, which are segmented and repeatedly mapped to the corresponding segments on the sides of a rectangle in the transformed domain. The segments forming the four corners of the original region in the physical domain must meet at right angles so as to map to right angles in the transformed domain. The x and y coordinates of the interior grid points are the solutions of the following Laplace's equations:

$$\frac{\partial^2 x}{\partial \xi^2} + \frac{\partial^2 x}{\partial \eta^2} = 0 \quad (3)$$

$$\frac{\partial^2 y}{\partial \xi^2} + \frac{\partial^2 y}{\partial \eta^2} = 0 \quad (4)$$

A Poisson solver is used to solve the equations, with the mapped boundary points providing the boundary conditions.

Given an open channel having one wall as in Fig. 3a, one side of the grid mesh is chosen to be on the curved wall. For simplicity, the other sides can be chosen to enclose a region of a fixed height. For an enclosed flow with two sidewalls visible in the image, both sidewalls can be used to generate the grid mesh. The maximum grid spacing in the physical domain should not be larger than image pixel size to avoid lost of intensity information during image interpolation. In fact, subpixel spacing can be used to reduce the peak-locking effect by applying correlation function with sub pixel window shift (Nobach et al. 2005). The mesh in Fig. 3b is generated using SeaGrid [developed from Gridpak (Wilkin and Hedström 1998) by Denham (2000)]. Pixel intensities at grid points are then interpolated to produce the rectangular image as in Fig. 3c. Bicubic interpolation was used in this paper to perform image resampling in the conformal transformations [see Nobach et al. (2005) for a detailed study of different image interpolation schemes].

2.3 Calculating stack of line correlations

In standard PIV, a typical 2D correlation function applied to image templates I and I' from the first and second exposures can be expressed as:

$$C_{U,V} = \sum_{m=1}^{M} \sum_{n=1}^{N} (I_{m,n} - \overline{I}) \left(I'_{m+U,n+V} - \overline{I'}_{U,V} \right) \quad (5)$$

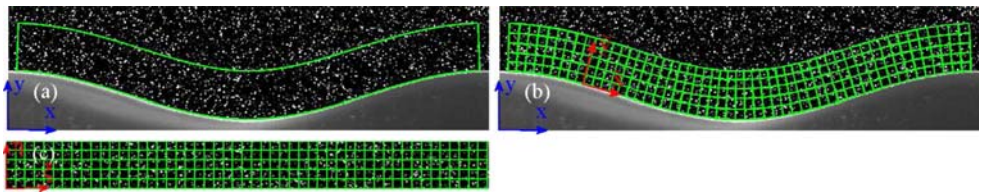

Fig. 3 Image transformation method to deal with curved walls. Given **a** curved boundary of near-wall region in (x, y) space, **b** orthogonal curvilinear grids are generated and for illustration purpose shown only 1 for every 20 grid lines. **c** Transformed near-wall image is obtained by a 2D interpolation. Previous local coordinate system $(\tilde{x}, \tilde{y})$ aligned to curved wall has been mapped to a rectilinear coordinate system (ξ, η)

where M and N are the template width and height (pixels), m and n the image coordinates (pixels), U and V are the displacement coordinates (pixels) of the resulting correlation map, $\overline{I}_{U,V}$ and $\overline{I'}$ are the mean values of the templates.

In this paper, to deal with near-wall flows, we propose a new 1D form of PIV correlation, named line correlation, that assumes a "quasi-tangential flow", i.e., where the interframe wall-normal displacement of tracers is less than the particle diameter, so that a purely tangential search can produce correlation peaks. Below is the formula of the "line correlation" function:

$$C_{U,n} = \sum_{m=1}^{M} \left(I_{m,n} - \overline{I}_n\right)\left(I'_{m+U,n} - \overline{I'}_{U,n}\right) \tag{6}$$

where $\overline{I}_n$ and $\overline{I'}_{U,n}$ are the mean intensities on each pixel line of the first and second template.

Figure 4 summarizes the procedure to calculate a stack of line correlations, as applied to a pair of synthetic image templates. The line correlation function in Eq. 6 is performed as follows: in the case $U = 0$, horizontal pixel line $I(1...M, n)$ at a vertical location n of the first template (1st exposure) is correlated horizontally with the line $I'(1...M, n)$ at the same height in the second template (2nd exposure). The correlation of each horizontal pixel line produces a 1D-correlation distribution. Grouping line-correlation distributions according to the vertical locations forms a 2D table $C_{U,n}$ that we refer to as "correlation stack". The peaks at a given height n within the correlation stack should lie at the horizontal positions corresponding to the tracers' horizontal displacements. This permits measurement of tangential velocity at single-pixel resolution in the wall-normal direction, i.e., it avoids the wall-normal averaging of correlation information within the image template by standard 2D correlation functions. The correlation function $C_{U,n}$ can be normalized by dividing by the r.m.s of $\left(I_{m,n} - \overline{I}_n\right)$ and the r.m.s of $\left(I'_{m+U,n} - \overline{I'}_{U,n}\right)$ to increase the correlation signal of weak particles. However, such normalization should be applied with care to low signal-to-noise ratio PIV images as it can amplify the noise. Subpixel interpolation of images before correlation

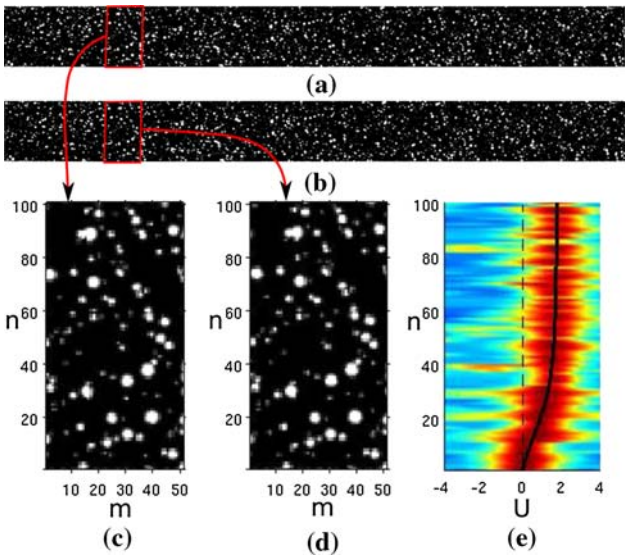

Fig. 4 Line correlation applied to a pair of synthetic image templates of near-wall flow (1 ms interframe delay). From a transformed near-wall image pairs (**a** and **b**) obtained as in Fig. 3, two image templates (**c** and **d**) of 50 × 100 pixels are extracted for measuring tangential velocity profile. Normalized line correlation applied to all horizontal pixel lines of the image templates produces a correlation stack (**e**) with the true displacement profile (DNS) shown as *black curve* overlaid on top. To reduce peak locking, transformed images were resampled at 0.1-pixel spacing to allow subpixel displacement in the line correlation. The distribution of the strong correlation forms a profile of the particle displacements which closely follow the theoretical distribution

is necessary to reduce the peak-locking error (Nobach et al. 2005) which can be a significant fraction of the small particle displacement near a wall. Subpixel interpolation can be done in the previous step during the conformal transformation by choosing subpixel grid spacing. The central-differential interrogation scheme (Wereley and Meinhart 2001) can also be applied to the correlation function, however, the accuracy improvement is minimal due to small displacement at the wall compared to the width of image template. An example of a normalized correlation stack obtained from a pair of image template with subpixel interpolation equivalent to 0.1 pixel is shown as an intensity map in Fig. 4e.

2.4 Integrating velocity profile

In our previous study (Nguyen and Wells 2006a), strong peaks were identified in a non-normalized correlation stack, and the velocity profile was fitted through these identified peak locations using Gaussian or spline interpolation. However, such a procedure is tedious and non-optimum; peak identification may reject correct but weak peaks, or accept strong false-peaks. In this paper, normalized correlation stack is recommended to obtain better measurement accuracy. Figure 5 shows the correlation peaks ('+' symbols) detected from a normalized correlation stack by searching for the horizontal position of the maximum correlation value at each pixel height. The peaks provide a noisy velocity measurement. The Gaussian interpolation, or Gaussian-weighted smoothing, (black curve) from the peak locations gives a much better velocity profile, although some deviations still exist. A small improvement can be achieved if the Gaussian smoothing is additionally weighted by the correlation peak intensities. To improve upon individual peak detection and interpolation (Nguyen and Wells 2006a), the present study proposes to extract the profiles of tangential velocity by incrementally fitting lines to the correlation stack as exemplified by the white curve in Fig. 5 and explained in Fig. 6a. By default, IPIV is used to call the measurement method using line fitting.

The new method does not require individual peak detection. The velocity profile is obtained by integrating the velocity gradient one pixel at a time in the wall-normal direction, which builds strong validation into the procedure. At each height, velocity gradient is extracted from the correlation stack by fitting a line through the correlation peaks.

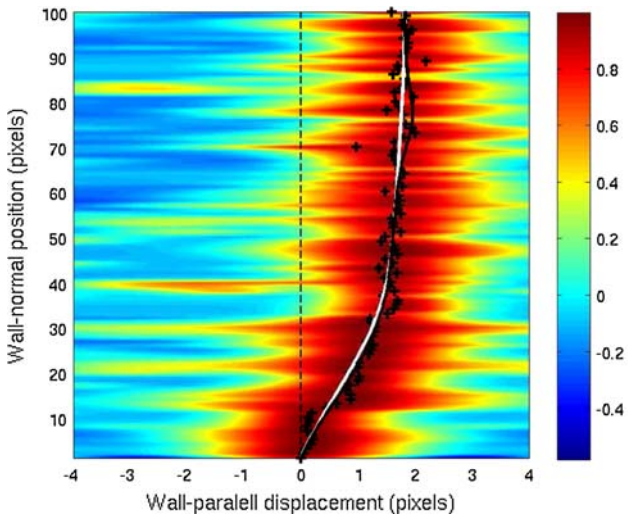

Fig. 5 Possible velocity measurement methods from correlation stacks (*colormap*) in IPIV. '+' symbols shows correlation peaks detected. *Black curve* shows the Gaussian interpolation from the detected peak. *White curve* shows incremental line fitting which is the recommended method in this paper

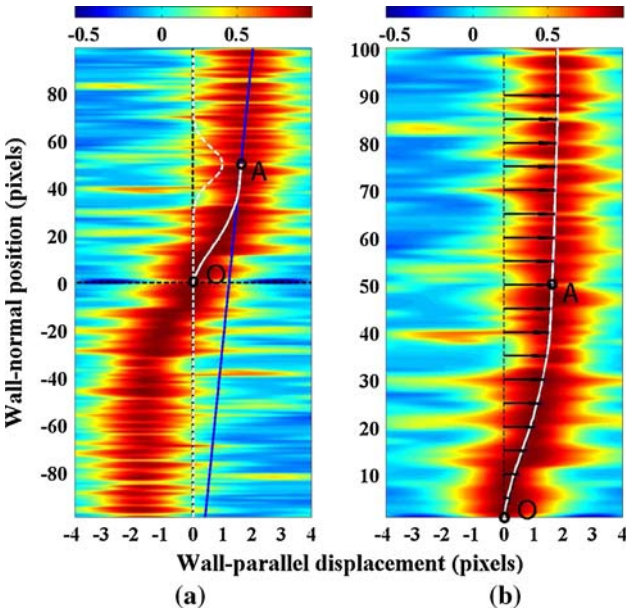

Fig. 6 Velocity interpolation method applied to the synthetic image templates in Fig. 4. Color maps are instantaneous normalized correlation stacks produced by line correlation (Eq. 6) from one template of a synthetic image pair. **a** The combined correlation stack consists of the original correlation stack on top of its 180°-rotated copy. The tangential velocity profile (*white curve*) is obtained by integrating velocity gradient, starting at point O at the wall. At point A, at which $n = 50$ pixels, Gaussian-weighted (*white dash curve*; $\sigma = 7$ pixels) line fitting yields the *solid black line*. **b** The whole velocity profile extracted from the same correlation stack by IPIV (*solid white curve*) compared with displacement vectors found by PID with template height of 11 pixels (*black vectors*) and the true profile (*black dashed curve*) from the imposed DNS snapshot (cf. Sect. 3)

Assuming no-slip $u(0) = 0$, this translates to:

$$u(n) = u(n-1) + \text{grad}(n) \tag{7}$$

where grad(n) is the gradient found at the wall-normal position n ($n = 0, 1... N$).

The velocity gradient grad(n) is taken equal to the slope of the fitting line along which the Gaussian-weighted sum of correlation values in Eq. 8 is maximal, i.e., $F(\text{grad}(n)) = F_{\max}$:

$$F(\text{grad}) \equiv \frac{\sum_{y=-N}^{N} C_{U,y}\Omega(y)}{\sum_{y=-N}^{N} \Omega(y)} \tag{8}$$

where U in $C_{U,y}$ is a function of (grad, y):

$$U(\text{grad}, y) = u(n) + (y-n)\text{grad} \tag{9}$$

and where the Gaussian-weighting function $\Omega(y)$ is centered at the current wall-normal position n:

$$\Omega(y) = \exp\left[-\frac{(y-n)^2}{2\sigma^2}\right] \tag{10}$$

The Gaussian weighting acts as a mask to reduce the measurement uncertainty (Gui et al. 2001), for this case, in

the vertical direction. The correlation values $C_{U,y}$ along the fitting line are obtained by 2D (bicubic) interpolation of the correlation stack. Near the wall, the fitting line includes the values from a rotated copy of the correlation stack around the wall location to impose no-slip. Fig. 6a shows the velocity gradient measurement at point A ($n = 50$ pixels). The Gaussian-weighting distribution (white dashed curve) with standard deviation (STD) $\sigma = 7.07$ pixels is plotted on the correlation stack (top half) combined with its rotated copy (bottom half). Correlation values along a straight line (solid black line) passing through A are accumulated with the Gaussian weighting function $\Omega(y)$. The slope of the line that maximizes the correlation summation (Eq. 8) is taken to be the measured velocity gradient. Compared to Nguyen and Wells (2006a), the shear velocity gradient at the wall, referred to as "wall-shear", is no longer separated from the determination of the velocity profile; rather it is simply the first step in our integration process from point O, which is fixed by the no-slip condition.

In case the no-slip condition is not satisfied, velocity integration can start from the top of the correlation stack where the velocity gradient is small and the velocity can be measured at high accuracy. Though we do not present data here, our tests have verified that integrating toward a slip boundary can yield accurate results for correlation stacks with high signal-to-noise ratio. For a no-slip condition, our tests have shown that the integration starting from the top of the correlation stack provides very similar tracer displacements, differing by a maximum of roughly 0.005 pixels just adjacent to the wall, when compared to the integration starting from the wall position.

In our particular test case, IPIV with normalized correlation produces better measurement accuracy than non-normalized correlation (not shown in this paper). As seen from Fig. 6b, the measurement with Gaussian STD $\sigma = 7$ pixels yields a plausible profile (white curve) that is very close to the true profile (black dash) based on DNS. A profile computed with $\sigma = 3.5$ pixels, Fig. 7a, is affected by small-scale noise from the correlation stack. On the other hand, the profile for $\sigma = 14$ pixels, shown in Fig. 7b, follows closely to the true profile, except in the region from 20 to 40 pixel where the profile bends most. In this test, IPIV successfully produces the velocity profiles up to 100-pixels height. As the friction Re based on wave amplitude (110 pixels) is 106 for the DNS flow, the height of the obtained velocity profile is equivalent to about 100 wall units.

2.5 Reverse transforming to physical domain

The relation between physical displacement (u, v) and the corresponding displacement (U, V) in the conformal transformed domain can be expressed as:

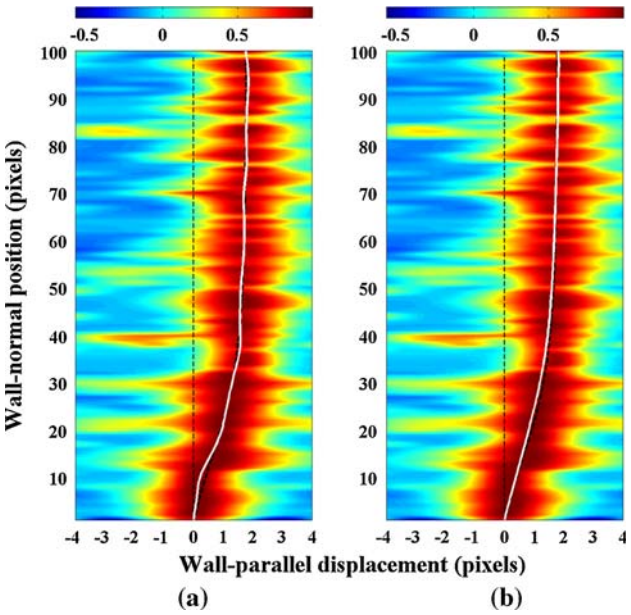

Fig. 7 The effect of varying the STD σ of the Gaussian-weighting function on measurement results for the synthetic image templates in Fig. 4. The detected velocity profile of IPIV (*white curve*) is plotted on the correlation stack and compared with DNS profile (*black dashed curve*) **a** $\sigma = 3.5$ pixels **b** $\sigma = 14$ pixels

$$u = \frac{\partial x}{\partial \xi}U + \frac{\partial x}{\partial \eta}V \tag{11}$$

$$v = \frac{\partial y}{\partial \xi}U + \frac{\partial y}{\partial \eta}V \tag{12}$$

The coefficients that characterize the coordinate transformation are defined as:

$$g_\xi = \sqrt{\left(\frac{\partial x}{\partial \xi}\right)^2 + \left(\frac{\partial y}{\partial \xi}\right)^2} \tag{13}$$

$$g_\eta = \sqrt{\left(\frac{\partial x}{\partial \eta}\right)^2 + \left(\frac{\partial y}{\partial \eta}\right)^2} \tag{14}$$

In IPIV, only the wall tangential displacement component U is measured in the transformed domain. In this case, the second terms in Eqs. 11 and 12 disappear. In the physical domain, the resulting displacement vector $(\frac{\partial x}{\partial \xi}U, \frac{\partial y}{\partial \xi}U)$ turns out to be the local-tangential displacement component, denoted $\tilde{u}$, with respect to local coordinates $(\tilde{x}, \tilde{y})$ that are aligned with wall boundary in the physical domain. The magnitude of this component can be obtained as:

$$\tilde{u} = \sqrt{\left(\frac{\partial x}{\partial \xi}U\right)^2 + \left(\frac{\partial y}{\partial \xi}U\right)^2} = U g_\xi \tag{15}$$

Wall-shear gradient can be obtained as:

$$\frac{\partial \tilde{u}}{\partial \tilde{y}} = \frac{\partial U g_\xi}{\partial \eta\, g_\eta} \tag{16}$$

where $\frac{\partial U}{\partial \eta}$ is the wall-shear gradient obtained in the transformed domain.

Usually, the grid spacing in the transformed domain is chosen to be 1 unit, or $\xi_{i,j} - \xi_{i-1,j} = 1$ and $\eta_{i,j} - \eta_{i,j-1} = 1$, where i is the running index in the horizontal grid direction and j is the running index in the vertical grid direction. As a result, Eqs. 15 and 16 at grid point $(x_{i,j}, y_{i,j})$ can be obtained as:

$$\tilde{u}_{i,j} = U_{i,j}\sqrt{(x_{i,j} - x_{i-1,j})^2 + (y_{i,j-1} - y_{i,j})^2} \tag{17}$$

$$\frac{\partial \tilde{u}_{i,j}}{\partial \tilde{y}_{i,j}} = (U_{i,j} - U_{i,j-1})\frac{\sqrt{(x_{i,j} - x_{i-1,j})^2 + (y_{i,j} - y_{i-1,j})^2}}{\sqrt{(x_{i,j} - x_{i,j-1})^2 + (y_{i,j} - y_{i,j-1})^2}} \tag{18}$$

where $U_{i,j}$ is the tangential displacement at grid point $(\xi_{i,j}, \eta_{i,j})$ in the transformed domain, and correspondingly $\tilde{u}_{i,j}$ is the tangential displacement at grid point $(x_{i,j}, y_{i,j})$ in the physical domain.

If stereo cameras are utilized, another step of stereo reconstruction of the wall-shear gradients, as described in our previous work (Nguyen and Wells 2006b), is required to obtain the physical wall-shear gradients.

To confirm that the method works with real images, we have performed a simple test in which a block, whose upper surface was machined to a sinusoid, was placed on the lower wall of an open channel as shown in Fig. 1. After applying IPIV, a tangential velocity profile is obtained as in Fig. 8. The figure shows a sample of instantaneous profiles of tangential displacement overlaid onto a near-wall region of 1,008 × 400 pixels which is cropped from a full 1,000 × 1,008 pixel image. The maximum displacement in the full image is about 10 pixels. Flow separation and reattachment are clearly evident. Reynolds number of the incoming flow is about 300, based on the wall-shear stress. To demonstrate that IPIV is fairly robust, the examples herein consider a region 100 pixels above the wall. But as confirmed in the following section, IPIV yields superior results mainly within a rather thin layer adjacent to the wall. To handle separating flow at higher Reynolds number, it should suffice to specify a suitably thin region for IPIV processing, within which the condition on wall-normal tracer displacement is satisfied; standard processing could be applied elsewhere.

As another application of IPIV to real flows, the reader is referred to Buchmann et al. (2008), in which wall-shear gradient was measured in a model of human carotid artery with and without a stenosis. This flow is characterized by clear separation and reattachment, with a maximum Reynolds number of 800, based on the flow velocity and the artery diameter at the model entrance. As a second example, Nguyen (2007) applied IPIV successfully to measure the wall-shear gradient of a reattaching flow downstream of a backstep at a Reynolds number Re = 2200, based on the free stream velocity and the step height. Although these flows are all characterized by rather low Re, IPIV should work at higher Reynolds number if sufficient camera resolution is employed; this is strictly analogous to the tradeoff between resolution and field of view that faces standard PIV away from walls at high-Reynolds number.

3 Validations of IPIV technique using synthetic images

IPIV have been designed to better deal with velocity measurements of flows in the vicinity of inclined or curve walls. Our tests (not shown in this paper) have shown that conformal transformation alone can provide 3 times better accuracy than centroid-shifting technique in velocity gradient measurements. The rest of the paper will focus on the performance validation of IPIV in directly resolving velocity gradient and velocity profiles near walls when compared to Particle Image Distortion (PID) technique performed on the same set of transformed images.

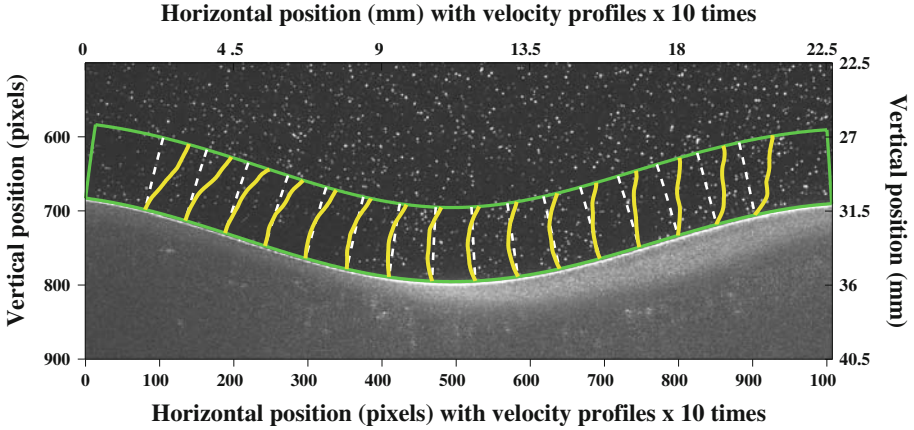

Fig. 8 Detected instantaneous profiles of tangential tracer displacement × 10 times by IPIV processing of experimental image data. Reynolds number of the incoming flow is around 300 based on the incoming wall-shear velocity. Maximum particle displacement far from wall is about 10 pixels. There is no overlapping between adjacent templates used for line correlation

3.1 Method

Basically, PID technique was applied in place of steps 3 and 4 of IPIV to obtain velocity measurements and the results were compared to those of IPIV. In addition to line fitting and velocity gradient integration in IPIV, two other schemes were also used to measure velocity profile (replacing step 4): (a) using correlation peak detection (PD) and (b) correlation peak detection with Gaussian interpolation (PD & GI), as previously shown in Fig. 5. The same Gaussian STD was used for both PD & GI and Gaussian weighting in IPIV (using line fitting).These measurement results were also included in the comparison of velocity measurements.

Synthetic images were generated from a single snapshot of a 3D DNS velocity field of a turbulent open-channel flow over a sinusoidal bed (Nakayama et al. 2002 and Yokojima 2002) that was characterized by flow separation and reattachment. The computational domain had 192 $\times$ 128 $\times$ 96 grid lines in the stream, span, and upward directions. The ratio between the wave peak-to-peak amplitude δ and the wave length λ was 0.05, giving a maximum wall slope of 0.31. The bulk Reynolds number based on the average velocity and the flow depth was 6,760. The Reynolds number based on friction velocity and peak-to-peak height is 106. The flow domain consisted of three wavelengths. Synthetic images were generated from the flow region corresponding to the central wavelength.

Eight-bit gray-scale images were generated following Lecordier et al. (2004). Tracers of non-uniform diameters were randomly scattered into a virtual 3-dimensional volume corresponding to a laser sheet of Gaussian intensity profile with $\sigma = 0.5$ mm or about 10 wall units. The tracer diameter varied from 2.2 to 6 pixels according to Gaussian distribution, with mean diameter = 2.8 pixels and $\sigma = 1.28$ pixels. The first simulated exposure captured the projection of the initial tracer positions. After a delay Δt, the second exposure again captured the projected tracers displaced according to spatial interpolation of the 3D velocity fields. Random background noise was generated with a Gaussian distribution with $\sigma = 2.5$ grayscale units. The minimum and maximum background levels were 30 and 45 gray-scale units, matching our experimental images. Seeding density in the resulting synthetic images was about 0.01 particle/pixel. Maximal tracer displacements was only 4.75 pixels, i.e., to guarantee that the wall-normal displacement of all particles in the whole image template is smaller than the mean particle diameter. Forty synthetic image pairs of 1,008 $\times$ 1,008 pixels were generated covering a field of view of $H \times H$, where H is the maximal flow depth, taken to be 50 mm. All PIV interrogations used the same template width $M = 50$ pixels.

In the transformed images, PID was performed on regularly spaced templates, the first having its bottom edge on the wall. Wall-shear gradient was obtained by dividing the measured velocity by the distance from the template center to the wall. Grid spacing of PID on transformed templates is 5 pixels in vertical and 25 pixels in horizontal directions. The interrogation window size was 50 $\times$ 11 pixels with 50% overlap between horizontally and vertically adjacent windows. To achieve convergence in PID, the interrogation window size had to be varied suitably, i.e., the template height was reduced to 8 pixels at the wall to handle the smaller displacements there, and a Gaussian-smoothing scheme analogous to step 4 was applied along streamwise and wall-normal directions to suppress the instability of PID iterations.

To quantify the velocity measurement errors, a random error ϵ_{rand} is defined as the r.m.s of the differences between $u(n)_p^q$ and their ensemble average and expressed as:

$$\epsilon_{\text{rand}} = \sqrt{\frac{1}{NPQ}\sum_{n=1}^{N}\sum_{q=1}^{Q}\sum_{p=1}^{P}\left(u(n)_p^q - \overline{u(n)}^q\right)^2} \tag{19}$$

where $Q = 38$ is the number of streamwise stations of measurement, $P = 40$ is the number of velocity fields obtained from 40 synthetic image pairs generated from the same DNS velocity field, N is the height of image template/correlation stack, and ensemble-averaged velocity $\overline{u(n)}^j$ is calculated as:

$$\overline{u(n)}^q = \frac{1}{P}\sum_{p=1}^{P} u(n)_p^q \tag{20}$$

A total error ϵ_{total} is defined as the r.m.s of the difference between $u(n)_p^q$ and the true velocity $U(n)^q$ based on DNS and expressed as:

$$\epsilon_{\text{total}} = \sqrt{\frac{1}{NPQ}\sum_{n=1}^{N}\sum_{q=1}^{Q}\sum_{p=1}^{P}\left(u(n)_p^q - U(n)^q\right)^2} \tag{21}$$

Similar total error for velocity gradient measurements can be obtained by Eq. 21 by replacing $u(n)_p^q$ by $\text{grad}(n)_p^q$, and $U(n)^q$ by its gradient.

3.2 Results and discussion

First, velocity gradient measurements are compared between the proposed IPIV (using line fitting) and PID. Figure 9 shows the measurement results along the wall by PID (triangles) and by IPIV (diamonds) along with the true values by DNS (squares). The error bars show the standard deviations of the measurements. Generally, the gradient measurements of both IPIV and PID agree well with the exact values. However, IPIV provides better agreement where there is a significant spatial variation of the gradient

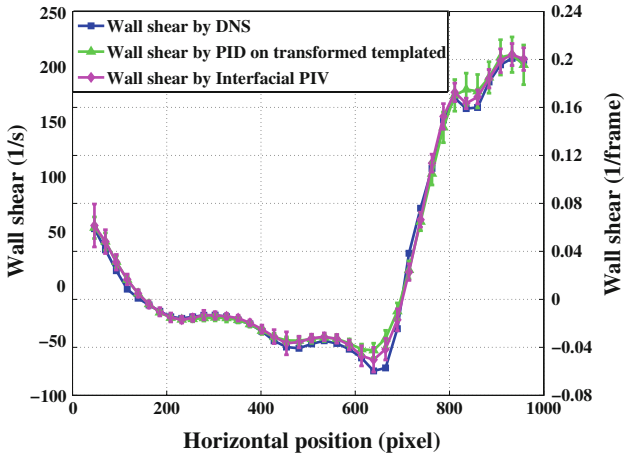

Fig. 9 Wall-shear measurement by IPIV versus PID for interframe time delay = 1 ms, yielding a maximum displacement of about 4.75 pixels. PID used template height = 11 pixels and IPIV used $\sigma = 7$ pixels, Wall-shears from DNS data (*squares*) compared to sample averages from processing 40 synthetic images pairs processed by PID on transformed rectangular images (*triangles*) and by IPIV (*diamonds*). Half-height of error bar corresponds to sample standard deviation of measured values at each position. The r.m.s. of the gradient difference between DNS data and the sample averages of PID on transformed templates is 1.289 s^{-1} and that of IPIV is 0.916 s^{-1}

along the wall. IPIV produces an accuracy improvement of 25% when compared to PID with the total errors ϵ_{total} of 0.916 s^{-1} and 1.289 s^{-1} respectively.

A quick comparison of velocity measurements between PID and IPIV was shown previously in Fig. 6b. In our implementations, IPIV provides a continuous velocity profile (white curve), whereas PID provides velocity vectors (arrows) at 5-pixel intervals in the wall-normal direction. Near the wall, below $n = 30$ pixels, IPIV provides measurement results closer to the true values from DNS snapshot than PID.

A more detailed comparison between results by PID and IPIV of different schemes of velocity measurements is shown in Fig. 10 for measurement points within $N = 15$ pixels from the wall. Comparable, near-optimal conditions were used for each method, i.e., template height of PID is 11 pixels and the Gaussian STD, σ, for IPIV 7.07 pixels. For IPIV, "full width at half maximum" (FWHM) is defined as 2.35 σ which is the most standard width descriptor for the purpose of comparing with the template height of PID. The same template width of 50 pixels and the horizontal search size of 8 pixels were used in both PID and IPIV. The data points represent ensemble-averaged tangential velocities.

Measurements by PID, Fig. 10a, and IPIV using peak detection (PD), Fig. 10b, yield significant deviations from the true velocity with the total errors $\epsilon_{\text{total}} = 0.161$ and 0.209 pixel, respectively. By applying Gaussian interpolation to the the detected peaks, IPIV can reduce half of the total error ($\epsilon_{\text{total}} = 0.088$ pixel) as shown in Fig. 10c. A further 10% of error reduction, not shown here, was found by additionally using the peak intensities as weights in Gaussian interpolation. Finally, IPIV using the recommended line fitting (LF) and gradient integration provides the smallest error ($\epsilon_{\text{total}} = 0.052$ pixel) as shown in Fig. 10d, equivalent to 1/3 of the total error by PID.

The effect of STD σ of Gaussian weighting in IPIV is similar to that of template height in normal PIV (cf. Fig. 7). If the Gaussian STD or template height (or size) is too small, random error is large. If the Gaussian STD or template height is too large, error due to low-pass filtering becomes significant. Fig. 11 shows PID measurements for template heights from 7, 9, 11, 13, 15, 17, and 19 pixels (to maintain PID templates within the fluid region, however, the height of the templates closest to the wall, $Y = 5$ pixels, is bounded at 8 pixels). The smallest random error and total error are achieved when template size is around 11 pixels. One sees that random error consistently decreases with increasing Gaussian STD σ between 3.5 and 14 pixels. However, the total error increases monotonically for the tested range of σ. This is explained by the fact that the error due to low-pass filtering also increases with σ. Overall, the total error of IPIV is smaller than that of PID, and can be made 40% lower by reducing σ sufficiently. In other words, IPIV offers greater resolution than PID adjacent to a fixed wall. Furthermore, IPIV avoids the inherent convergence problem present in PID. The total error ϵ_{total} obtained for $\sigma = 3.5$ pixels is less than 0.1 pixel, which suggests that the velocity profile adjacent to the wall by IPIV could be attained with sub pixel accuracy.

Away from the wall, we have compared results from PID and IPIV analogously to Fig. 11, for measurement points between 16 and 100 transformed pixels above the wall. For both IPIV and PID, the total error is essentially constant at 0.18 pixels, except that a template height of 13 pixels or greater for PID yields a substantially higher total error, and we conclude that IPIV affords comparable accuracy to PID away from the wall. To reiterate, however, IPIV is conditional on wall-normal tracer displacement being less than the diameter of the tracer images.

As a rough guide, we suggest that the optimum value of σ roughly corresponds to about 7 wall units, as follows. For the near-wall region, Fig. 11 suggests that $\sigma = 3.5$ pixels is the best choice, while analogous data for the region above 16 pixels mentioned in the last paragraph (not shown) suggest a very weak minimum at 7 pixels. As a practical matter, a comparison of the profiles generated for these two choices in Fig. 6b ($\sigma = 7$ pixels) and Fig. 7a ($\sigma = 3.5$ pixels) would lead most practitioners to choose the larger value. This value of σ, 7 pixels, roughly corresponds to about 7 wall units of the flow. In these tests, seeding density was 0.01 particle/pixel, which translates to

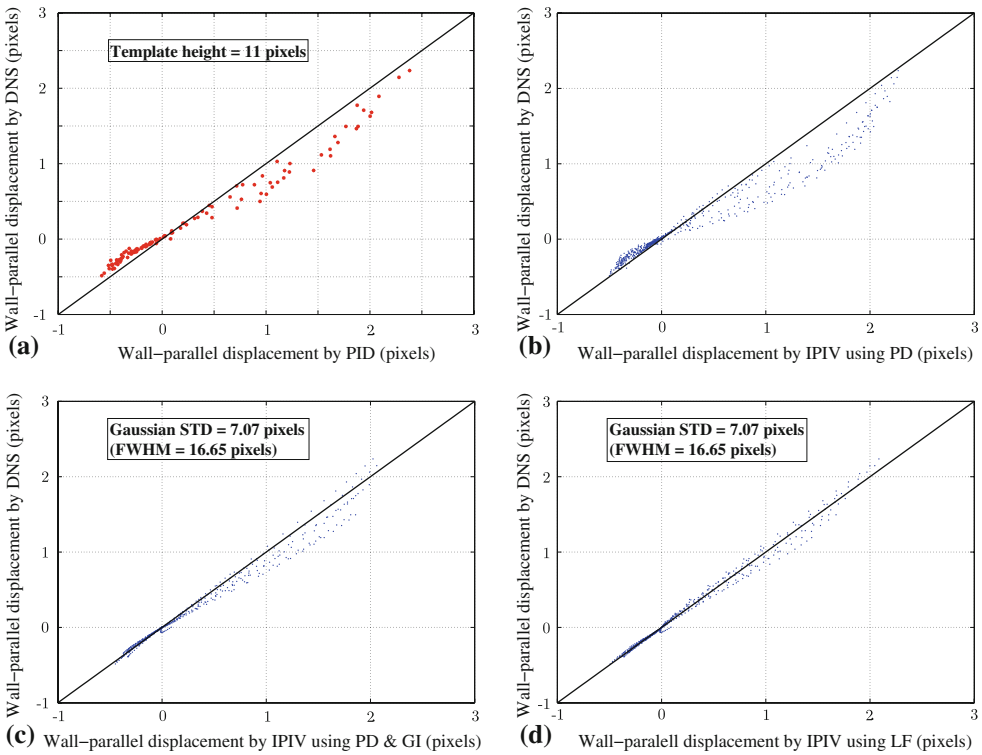

Fig. 10 Point-to-point comparisons of displacement measurements in the transformed domain against those by DNS, from 40 synthetic image pairs for measurement points within 15 pixels from wall. **a** PID with template height = 11 pixels applied to transformed images resulting in $\epsilon_{\text{total}} = 0.161$ pixel). **b** IPIV using peak detection (*PD*) resulting in $\epsilon_{\text{total}} = 0.209$ pixel, and **c** IPIV using peak detection and Gaussian interpolation (PD & GI) with $\sigma = 7.07$ pixels resulting in $\epsilon_{\text{total}} = 0.088$ pixel and a further 10% error reduction if used peak intensity as weighting. **d** IPIV using line fitting (*LF*) recommended in this paper with $\sigma = 7.07$ pixels resulting in $\epsilon_{\text{total}} = 0.052$ pixel. The *straight lines* indicate zero error location

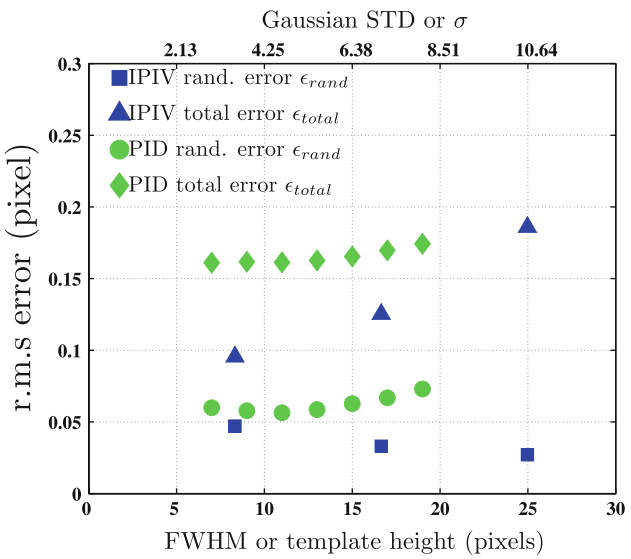

Fig. 11 Root mean square errors of velocity measurements, expressed as interframe pixel displacement, by PID and IPIV with increasing template height or Gaussian STD, σ, for measurement points within 15 pixels from wall. The random and total errors of PID are minimum around template height of 11 pixels. From $\sigma = 3.5$ pixels, the random error of IPIV decreases with increasing σ, while the total error increases monotonously. Overall, IPIV produces significantly smaller total error than PID for the same FWHM and template width. One pixel is equivalent to 1 wall unit

3.5 particles in a region of (template width) $\times$ σ. Higher seeding density should allow smaller σ and higher measurement accuracy.

4 Conclusions

This paper has presented IPIV, an approach for extracting accurate wall-shear gradient and detailed near-wall profiles of tangential velocity. The method comprises a conformal transformation to straighten images at a curved wall (or just realign pixels to a straight but inclined wall), a novel 1D cross-correlation and a novel velocity integration. Tangential velocity gradient now is simply obtained from the first step in our velocity integration process. The capability of our line correlation and velocity integration has been successfully tested with real images from separating flow over a wavy bed, and benchmarked against the PID technique using realistic synthetic images. The velocity and velocity gradient measurements by IPIV using line fitting and velocity gradient integration provide better agreement with true values than data from the PID technique and IPIV using peak detection with/without Gaussian interpolation. The optimum STD of Gaussian weighting roughly corresponds to 7 wall units, and the measurement accuracy varies only slightly with the selection of the Gaussian STD. IPIV is non-iterative, and thus more tractable than iterative PIV which often entails convergence problems. We have also demonstrated that the conformal transformation can be independently utilized by a standard PIV method, such as PID. Although IPIV is applicable only in the region where wall-normal particle displacement is smaller than the particle diameter, our test suggests it can produce an accurate velocity profile over a distance equivalent to about 100

wall units from the wall if interframe delay is shortened sufficiently. The method should be valuable in applications to complex, separating boundary flows, such as the flow over a sinusoidal wall presented in this paper or the flow in a modeled carotid artery (Buchmann et al. 2008, 2009).

Acknowledgments The first author would like to express appreciation to Dr. Frédéric Plourde, Laboratoire d'Etudes Thermiques—ENSMA, Poitiers, France, for his challenging question about how to deal with curved walls. We also express our special thanks to Nicolas Buchmann, Department of Mechanical Engineering, University of Canterbury, New Zealand, for his valuable discussion on our technique. We acknowledge Charles Denham's generosity for making SeaGrid toolbox freely available.

References

Buchmann NA, Nguyen CV, Wells JC, Jermy M (2008) In-vitro wall-shear stress measurements using interfacial particle image velocimetry (IPIV). In: 14th International symposium on applications of laser techniques to fluid mechanics, Lisbon, 07–10 July

Buchmann NA, Jermy MC, Nguyen CV (2009) Experimental investigation of carotid artery haemodynamics in an anatomically realistic model. Int J Exp Comput Biomech 1(2):172–192

Denham CR (2000) SeaGrid orthogonal grid maker for Matlab. Woods Hole Science Center, U.S. Geological Survey. http://woodshole.er.usgs.gov/operations/modeling/seagrid/

Gui L, Merzkirch W, Fei R (2000) A digital mask technique for reducing the bias error of the correlation-based PIV interrogation algorithm. Exp Fluids 29(1):30–35

Gui L, Longo J, Stern F (2001) Biases of PIV measurement of turbulent flow and the masked correlation-based interrogation algorithm. Exp Fluids 30:27–35

Hochareon MB, Fontaine A (2004) Wall-shear-rate estimation within the 50cc Penn State artificial heart using particle image velocimetry. J Biomech Eng 126:430–437

Huang HT, Fiedler HE, Wang JJ (1993) Limitation and Improvement of PIV. Exp Fluids 15:263–273

Ives DD, Zacharias RM (1987) Conformal mapping and orthogonal grid generation. AIAA/SAE/ASME/ASEE 23rd joint propulsion conference, Paper No. 87-2057, San Diego

Lecordier B, Westerweel J (2004) The EUROPIV synthetic image generator (S.I.G.). In: Particle image velocimetry: recent improvements. Proceedings of the EUROPIV 2 workshop held in Zaragoza, March 31 April 1, 2003. Springer, Heidelberg

Marr D, Hildreth E (1980) Theory of edge detection. In: Proceedings of the Royal Society of London, Series B, Biological Sciences 2007, pp 187–217

Nakayama A, Sakio K (2002) Simulation of flows over wavy rough boundaries. Center for Turbulent Research, Annual Research Briefs: pp 313–324

Nguyen TD (2007) Development of Stereo PIV: application to turbulent flow over a backward-facing step. Masters thesis, Ritsumeikan University, Shiga

Nguyen CV, Wells JC (2006a) Development of PIV/interface gradiometry to handle low tracer density and curved walls. In: Proceedings of FEDSM2006 European fluids engineering summer meeting, Miami

Nguyen CV, Wells JC (2006b) Direct measurement of fluid velocity gradients at a wall by PIV image processing with stereo reconstruction. J Vis 45:5–27; adapted from Nguyen CV, Phan NMT, Wells JC (2004) Proceedings of international conference on advanced optical diagnostics in fluids, solids and combustion, Tokyo

Nguyen CV, Nguyen TD, Wells JC (2006) Sensitivity of PIV/interface gradiometry to estimated wall position. J Vis Soc Jpn 26(2):203–206

Nobach H, Damaschke N, Tropea C (2005) High-precision sub-pixel interpolation in particle image velocimetry image processing. Exp Fluids 39:299–304

Theunissen R, Scarano F, Riethmuller ML (2008) On improvement of PIV image interrogation near stationary interfaces, Exp Fluids (online)

Wereley ST, Meinhart CD (2001) Second-order accurate particle image velocimetry. Exp Fluids 31(3):258–268

Westerweel J, Geelhoed P, Lindken R (2004) Single-pixel resolution ensemble correlation for micro-PIV applications. Exp Fluids 37:375–384

Wilkin J, Hedström KS (1998) User's manual for an orthogonal curvilinear grid-generation package. Institute of Marine and Coastal Sciences, Rutgers University http://www.marine.rutgers.edu/po/tools/gridpak/grid_manual.ps.gz

Yokojima S (2002) Modeling and simulation of turbulent open-channel flows emphasizing free-surface effects. PhD thesis, Kobe University, Kobe